Journal of Catalysis **206,** 202–217 (2002)
doi:10.1006/jcat.2001.3506, available online at http://www.idealibrary.com on IDEAL®

Promoted Iron-Based Catalysts for the Fischer–Tropsch Synthesis: Design, Synthesis, Site Densities, and Catalytic Properties

Senzi Li,* Sundaram Krishnamoorthy,* Anwu Li,* George D. Meitzner,† and Enrique Iglesia*,[1]

*Department of Chemical Engineering, University of California at Berkeley, Berkeley, California 94720-1462; and †Edge Analytical, Inc., Middleton, Wisconsin 53562

Received May 17, 2001; revised December 26, 2001; accepted December 28, 2001

Iron-based catalysts were prepared by using promoters (K, Ru, Cu) and synthesis and activation protocols that inhibit sintering of oxide precursors and favor the nucleation of small Fe carbide crystallites. The effects of promoters on reduction/carburization behavior, on Fischer–Tropsch synthesis (FTS) rates, and on the number of CO binding sites formed during reaction were examined by combining steady state and transient rate measurements, titration of active sites, and X-ray absorption spectroscopy. K, Ru, and Cu promoters increased reduction/carburization rates of Fe–Zn oxide precursors, steady-state FTS rates, and the number of CO binding sites present after activation and FTS. These promoters increased the number of active sites formed during activation by favoring the nucleation of smaller Fe_3O_4 and FeC_x domains as Fe_2O_3 precursors were transformed into active catalysts during initial contact of oxide precursors with synthesis gas. These smaller crystallites, in turn, provide higher surface areas, a larger number of CO binding sites, shorter distances for lattice oxygen diffusion during carburization, and higher steady state FTS rates. The use of surface-active alcohols during drying and thermal treatment of oxide precursors also led to higher active site densities and FTS rates; these methods minimized sintering of oxide precursors during these thermal treatments. Turnover rates on Fe-based catalysts were about three times lower than on Co-based catalysts, at conditions typical used for the latter (473 K, 2.0 MPa). Hydrocarbon synthesis rates (per catalyst mass or volume) on Fe–Zn–Cu–K catalysts prepared by the methods described here were similar to those on representative Co-based catalysts at these conditions. Fe–Zn–Cu–K catalysts gave much lower CH_4 selectivities than Co-based catalysts. Fe-based catalysts also showed much weaker effects of temperature and of synthesis gas composition on CH_4 and C_{5+} selectivities. CO_2 selectivities were lower than on previous Fe-based catalysts, predominately because of the lower reaction temperatures made possible by the high active site densities attained on the promoted Fe–Zn catalysts reported in this study.

INTRODUCTION

Fe-based catalysts provide an attractive complement to Co-based catalysts for the Fischer–Tropsch synthesis (FTS). They lead to more olefinic products and to lower CH_4 selectivities than Co-based catalysts over a wide range of temperature and H_2/CO ratio, including synthesis gas streams with low H_2/CO ratios derived from coal or biomass (1). Cobalt catalysts are typically more active than Fe-based catalysts, but they require low reaction temperatures (470–490 K), because the selectivity to desired C_{5+} hydrocarbons and the quality of the diesel-range products formed become unacceptable at higher temperatures (2). The lower apparent FTS rates on Fe-based catalysts reflect to some extent the lower dispersion of their active components. Thus, an increase in the surface area and in the density of active sites during synthesis and during the initial stages of use in synthesis gas may bring Fe-based catalysts into the range of productivity and reaction conditions typical of Co-based catalysts (3). The resulting opportunities for using Fe-based catalysts at lower temperatures may also lead to even heavier products and to lower CO_2 selectivities. Such active Fe-based catalysts would also allow direct comparisons of FTS turnover rates on Fe and Co catalysts at similar conditions. Such comparisons require reliable measurements of the number of exposed active components in both catalysts. These measurements are available for Co catalysts, but not for Fe-based catalysts, which activate to form complex mixtures of oxide and carbide phases only during Fischer–Tropsch synthesis reactions.

Here, we report the design and synthesis of Fe-based catalysts with hydrocarbon synthesis productivities (per catalyst mass or volume) similar to those on Co-based materials. We also report direct comparisons of turnover rates on these two types of catalysts. These comparisons exploit a method developed to titrate the number of CO binding sites on Fe catalysts after activation and FTS reaction. Our previous studies of the catalytic properties of Fe (4) and Fe–Zn (5) catalysts have shown that FTS rates increased with K or Cu addition, and that the rate was highest when both K and Cu were present (6). These promotional effects reflect predominately the formation of Fe carbides with higher dispersion when K or Cu is present. Our initial attempt to improve the density of active sites in these materials and to decrease the CO_2 selectivity led us to replace Cu,

[1] To whom correspondence should be addressed. E-mail: iglesia@cchem.berkeley.edu.

0021-9517/02 $35.00

the active component in the best available water-gas shift (WGS) catalysts (7), with Ru. Ru was chosen because it does not introduce undesired methanation side reactions and it is an active, but impractical, FTS catalyst (8), and a promoter for Co-based catalysts (9). Ru increased FTS rates more effectively than Cu at similar atomic contents without detectable changes in chain growth selectivity. As in the case of Cu, Ru predominately increased the density of active sites by favoring the nucleation of smaller Fe carbide and Fe_3O_4 domains as Fe_2O_3 precursors convert to active catalysts during the initial stages of FTS reactions. This conclusion was confirmed by surface area, CO chemisorption, and isothermal transient experiments. These smaller crystallites, in turn, provided higher surface areas, shorter distances for diffusion of lattice oxygen during oxide-to-carbide transformations, more complete carburization of Fe_2O_3 precursors, and higher steady-state FTS rates.

Higher FTS rates were also achieved by synthetic protocols leading to higher precursor surface areas. These led to a higher Fe_2O_3 dispersion, which was maintained during catalyst activation in synthesis gas, when precursor decomposition and activation procedures were designed in order to minimize the subsequent sintering of these high surface area oxide precursors. FTS rates and selectivities were measured on these materials at reaction conditions typical of Co catalysts ($H_2/CO = 2$, 2.0 MPa, 473 K) on a high surface area Fe–Zn–K–Cu oxide catalyst and compared with those on Co/SiO_2 and $Co–Re/TiO_2$ catalysts previously reported (10, 27). The results reported here show that turnover rates are higher on exposed Co surface atoms than on Fe-based active sites. Fe-based catalysts designed with a high density of CO binding sites, however, can lead to similar and even higher hydrocarbon synthesis productivities and to lower CH_4 selectivities than Co-based FTS catalysts.

EXPERIMENTAL

Synthesis of Precursors and Catalysts

Fe–Zn oxide precursors were prepared by coprecipitation of oxyhydroxides from a mixed solution of Fe and Zn nitrates using ammonium carbonate. A solution containing $Fe(NO_3)_3$ (Aldrich, 99.9+%, 3.0 M) and $Zn(NO_3)_2$ (Aldrich, 99.9+%, 1.4 M) at a Zn/Fe atomic ratio of 0.1 was introduced into a large flask containing deionized water at 353 K (~100 cm^3) at a rate of 120 $cm^3\,h^{-1}$ using a liquid pump. A $(NH_4)_2CO_3$ (Aldrich, 99.9%, 1 M) solution was added separately into this flask at a rate required to maintain the pH at a constant value of 7.0 ± 0.1, measured by a pH meter (Omega, PHB-62). The precipitated powders (~20 g) were washed five times with doubly distilled deionized water (~200 cm^3/g each time), dried in ambient air at 393 K overnight, and then treated in flowing dry air at 623 K for 1 h. The K, Cu, and Ru promoters were added to these Fe–Zn oxide precursors by incipient wetness impregnation with aqueous solutions of K_2CO_3 (Aldrich, 99.99%, 0.16 M), $Cu(NO_3)_2$ (Aldrich, 99.99%, 0.16 M), or ruthenium (III) nitrosyl nitrate $[Ru(NO)(NO_3)_x(OH)_y$ $(x + y = 3)]$ (Aldrich, dilute nitric acid solution, Ru 1.5%) at the concentrations required to obtain the desired K/Fe, Cu/Fe, and Ru/Fe atomic ratios ($K/Fe = 0.02$, $Cu(Ru)/Fe = 0.01$). These impregnated samples were then dried 373 K in ambient air. Finally, the samples were treated in flowing dry air at 673 K for 4 h. The resulting oxide precursors are denoted throughout as $Fe–Zn–K_2$, $Fe–Zn–K_2–Cu_1$, and $Fe–Zn–K_2–Ru_1$, respectively. The subscripts denote the atomic content of the corresponding promoter divided by the Fe atomic content ($\times 100$).

High surface area Fe–Zn–K–Cu oxide precursors were prepared using a solvent replacement method. Alcohols, which have lower surface tension than water (11), were used to replace water in the precipitate washing steps in order to minimize pore pinching during subsequent drying. When intrapore liquids with high surface tension are removed by drying, the surface tension of liquids can cause pore mouth pinching and a loss of accessible pore volume and surface area (12–14). $Fe–Zn–K_4–Cu_2$ oxides were prepared by the procedure described above, except that alcohols (isopropanol or ethanol) were used to replace the water retained within pores during precipitation before the samples were dried. After coprecipitation, the powders were washed with isopropanol or ethanol (Fisher Chemical) five times (~200 cm^3/g each time) at ambient temperature. Magnetic stirring was used during alcohol washing in order to increase the rate at which liquid water within pores was replaced by the alcohol. In order to maintain similar promoter surface densities on these higher surface area oxides, proportionally higher concentrations of K ($K/Fe = 0.04$) and Cu ($Cu/Fe = 0.02$) were introduced during incipient wetness impregnation with the promoter salts.

A Co/SiO_2 catalyst (21.9 wt.% Co) was prepared by incipient wetness impregnation of SiO_2 (Grace-Davison; grade 62) with a solution of cobalt nitrate (Aldrich, 98%, 2.5 M), dried in ambient air at 333 K, and treated in H_2 using previously reported procedures (15). This sample showed a Co dispersion of 4.6% using H_2 chemisorption methods. Its FTS turnover rate at 473 K and 2.0 MPa was 46–73 h^{-1}, depending on the CO conversion level and the prevalent H_2O partial pressure. This performance places it among the Co-based catalysts with the highest reported turnover rates at these reaction conditions (10).

Fischer–Tropsch Synthesis Rate and Selectivity Measurements

FTS reaction rates and selectivities were measured on both Fe and Co catalysts using a fixed-bed single-pass flow reactor with plug-flow hydrodynamics. This reactor was held within a three-zone furnace controlled by three

temperature controllers (Watlow, Series 982 and 988). The tubular reactors were constructed of stainless steel (SS 304, 1.27 cm outer diameter and 1 cm inner diameter for Fe catalysts; 0.95 cm outer diameter and 0.5 cm inner diameter for Co catalysts). Axial temperature profiles were measured using a type K movable thermocouple contained within a 0.32 cm thermowell. The temperatures at all bed positions were within ±0.5 K of the average bed temperature. All lines after the reactor were kept at 433–553 K and a vessel placed immediately after the reactor was held at 408 K in order to collect liquid products. Another vessel was placed at ambient pressure and temperature after a sampling valve, which collected gaseous components (at ambient pressure and 523 K) for injection into a gas chromatograph.

Fe catalysts (100–180 μ, 0.4 g) were diluted with 11 g of quartz granules (100–180 μ) in order to avoid temperature gradients. These quartz granules were washed with concentrated nitric acid and treated in air at 973 K before use. Catalysts were activated using flowing synthesis gas ($H_2/CO = 2$) at 0.1 MPa by increasing the temperature from 298 to 423 K at a rate of 0.167 K/s and from 423 to 543 K at 0.017 K/s. The samples were held at 543 K for 1 h and the synthesis gas pressure was gradually increased to 2 MPa. The Co catalyst (100–180 μ, 1.06 g) was diluted with the SiO_2 support (3 g) used to prepare it and reduced again in pure H_2 (Airgas: 99.99% H_2, 0.538 mol/g-s) by increasing the temperature from 298 to 598 K at 0.167 K/s and holding at 598 K for 1 h. After reduction, the temperature was decreased to 473 K, synthesis gas was introduced, and the pressure was increased gradually to 2.0 MPa.

$H_2/CO/N_2$ mixtures (0.62/0.31/0.07 mol; Praxair: 99.9% H_2, 99.9% CO, 99.99% N_2) were used as reactants. N_2 was used as an internal standard in order to ensure accurate mass balances. This reactant mixture was purified using activated carbon (Sorb-Tech RL-13) in order to remove metal carbonyls and a molecular sieve trap (Matheson, Model 452A) in order to remove water. All flows were metered using electronic mass flow controllers (Porter, Model 201-AFASVCAA or Brooks, Model 5850-CAB1AF1A3). Reactant and product streams were analyzed online using a gas chromatograph (Hewlett Packard, Model 5890 Series II) equipped with a 10-port sampling valve and two sample loops. The contents of one sample loop were injected into a cross-linked methyl silicone capillary column (HP-1, 50 m × 0.32 mm; 1.05 μ film). The contents of the other loop were injected into a Porapak Q (15.2 cm × 0.318 cm) packed column. Ar, N_2, CO, CO_2, and light hydrocarbons eluting from the packed column were analyzed using a thermal conductivity detector (TCD). A flame ionization detector (FID) was used to analyze all hydrocarbon products as they eluted from the capillary column. The concentrations of all hydrocarbons up to C_{15} were measured using these chromatographic protocols.

Temperature-Programmed Reduction/Carburization of Fe–Zn–K–Cu(Ru) Oxides Using H_2 or CO

The reduction and carburization kinetics of promoted Fe–Zn oxide precursors were measured using temperature-programmed reaction (TPR) methods with H_2 and CO as reactants. Samples (0.2 g, 100–180 μ) were placed within a quartz cell (10 mm i.d.), supported on a quartz frit as a thin packed bed, heated in 20% O_2/Ar (0.268 mol/h) to 673 K at 0.33 K/s, and held at 673 K for 0.2 h in order to remove H_2O before reduction or carburization experiments. These samples were then cooled to ambient temperature in Ar and the gas stream was switched to 20% H_2/Ar or 20% CO/Ar (0.268 mol/h). The sample temperature was then increased to 1000 K at 0.167 Ks^{-1}. A part of the effluent stream (∼40%) was diverted into a differentially pumped atmospheric sampling system connected to a quadrupole mass spectrometer (Leybold Inficon Instruments Co., Inc.) in order to measure the concentration of reactants (CO or H_2) and of any reduction or carburization products formed.

In Situ X-Ray Absorption Spectroscopy

Fe K-edge X-ray absorption spectra were measured at the Stanford Synchrotron Radiation Laboratory (SSRL) using a wiggler side-station (beamline 4-1). The storage ring was operated at 30–100 mA and 3.0 GeV. Two Si (111) crystals detuned by 20% in order to minimize harmonics were used as the monochromator. The intensities of the X-ray beam incident on the sample (I_0), after the sample (I_1), and after a 5 μ Fe foil (I_2), were measured using three N_2-filled ion chambers, and the sample (I_0/I_1) and reference (I_1/I_2) spectra were simultaneously obtained. The most restrictive aperture along the beam path was a 0.2 × 12 mm slit within the hutch, which gave a 2 eV energy resolution at the Fe K-edge (7.112 keV) (16). The catalyst samples (100–180 μ) were diluted to 10 wt% Fe using graphite powder (Alfa AESAR, 99.9995%, $S_g < 1$ m^2/g, 180–250 μ) and placed within a quartz capillary cell (4). The analysis of X-ray absorption data was carried out using WinXAS (version 1.2) (17). Calibration of raw spectra was achieved by the alignment of the first inflection point in the Fe foil spectrum with the known absorption energy of Fe^0 (7.112 keV). Background subtraction was performed using linear fits for the preedge region (6.900–7.100 keV) and a sixth-order polynomial normalization for the postedge region (7.240–8.120 keV). Principal component analysis (18) and linear combination methods (19) were used in order to calculate the relative abundance of the various Fe phases, using the near-edge spectral region between 7.090 and 7.240 keV. The approach used to identify and quantify Fe species formed during FTS reactions has been described elsewhere (4).

Isothermal Transient Measurements of Fischer–Tropsch Synthesis Reaction Rates

Isothermal transient experiments were used in order to obtain product formation rates during FTS at conditions identical to those leading to the structural changes detected during *in situ* X-ray absorption studies. Samples (0.2 g, 100–180 μ) were diluted with graphite (0.5 g, 180–250 μ, Alfa AESAR, 99.998%) and placed within a quartz microreactor. They were then treated in He (Matheson, 99.999%, 0.268 mol/h) at 573 K for 0.2 h and cooled to 523 K. The He stream was then replaced with synthesis gas at 523 K (H_2/CO/Ar : 0.40/0.20/0.40 mole fractions; 0.1 MPa; Matheson, 99.999%, 0.268 mol/h). The resulting transients in the rates of formation of various FTS products (e.g., CH_4, H_2O, CO_2, etc.) were measured as a function of time using online mass spectrometry. The rate of CH_4 formation was used as a surrogate measure of the total FTS rates, because it can be measured accurately, and it changes with time on-stream in parallel with the formation rates of higher hydrocarbons.

CO Chemisorption and Surface Area Measurements

Catalyst samples (0.2 g, 100–180 μ, diluted with graphite) were treated in flowing He (0.268 mol/h) up to 573 K and cooled to 523 K. The flow was then switched to synthesis gas (H_2/CO/Ar : 0.40/0.20/0.40 mol; 0.1 MPa; Matheson, 99.999%, 0.268 mol/h) at 523 K for 1 h. Reversibly adsorbed species were removed by flowing He (0.268 mol/h) at 523 K for 1 h. Following these steps, the samples were cooled to ambient temperature, and CO chemisorption uptakes and BET surface areas were measured.

Two types of CO temperature-programmed desorption (TPD) experiments were performed. In the first type, a flow of 20% CO/Ar (1 bar; 0.268 mol/h) was passed through the sample for 0.5 h. This was followed by the removal of weakly adsorbed species using Ar (Matheson, 99.999%, 0.268 mol/h) at ambient temperature for 0.5 h. The samples were then heated to 1000 K at 0.167 K/s and the rate of CO_x evolution ($CO + CO_2$) into the Ar flow (0.268 mol/h) was measured by mass spectrometry. The other type of measurement involved a similar procedure, but without a CO chemisorption step after FTS. The difference between the CO desorption peak areas in these two experiments was used to estimate the number of sites available for reversible CO chemisorption after activation and FTS reactions. This procedure ensured the accurate subtraction of any CO_x formed during desorption experiments from irreversibly adsorbed carbon species formed during FTS or by reactions of carbidic carbon with residual lattice oxygen from the total CO desorption peak.

BET surface area measurements were carried out after FTS reactions at 523 K and flushing with He (0.268 mol/h) at this temperature for 1 h in order to remove reversibly adsorbed species and residual FTS hydrocarbons. The sample was then cooled down and passivated in flowing 1% O_2/He at RT for 1 h before exposure to air. N_2 physisorption measurements were performed at its normal boiling point (77 K) using an Autosorb 6 system (Quantachrome, Inc.) and surface areas were calculated using the BET method.

RESULTS AND DISCUSSION

Comparison of the Reduction and Carburization Behavior of Fe–Zn–K Oxides Promoted with Ru or Cu

Figure 1 shows oxygen removal rates for Fe–Zn–K–Cu and Fe–Zn–K–Ru oxides as a function of temperature during exposure to flowing H_2. The amounts of oxygen removed in each of the two major reduction peaks indicate that the reduction of Fe–Zn–K–Cu(Ru) oxides follows the same sequential reduction steps observed for Fe_2O_3 (5). Fe_2O_3 reduces to Fe_3O_4 and then to Fe in two steps with distinct kinetics. The addition of Cu to Fe–Zn–K oxides led to incipient reduction at ~130 K lower temperatures than on Cu-free samples (Figs. 1a and 1b), as a result of H_2 dissociation sites formed by reduction of CuO to Cu metal at low temperatures. Ru had similar but stronger effects on the temperature required for reduction of Fe_2O_3 to Fe_3O_4 and of Fe_3O_4 to Fe (by an additional decrease of 50 and 100 K, respectively). It appears that Ru, because of its higher metal dispersion, lower reduction temperature, or higher H_2 dissociation turnover rate, leads to higher hydrogen

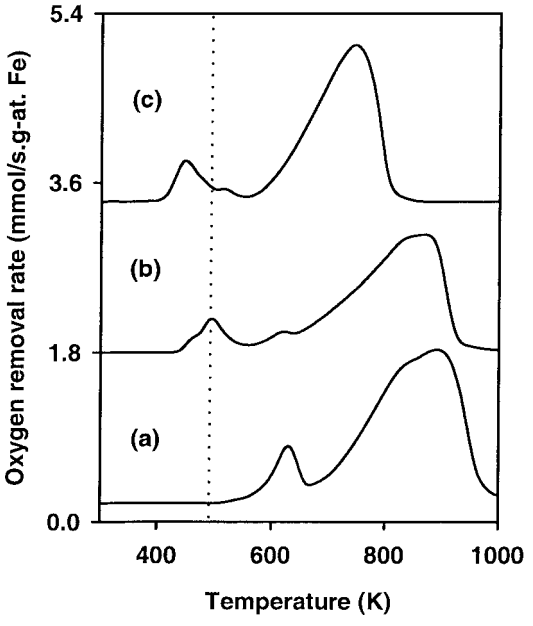

FIG. 1. Oxygen removal rates for Fe–Zn–K–Cu(Ru) oxides in H_2. (a) Fe–Zn–K_2, (b) Fe–Zn–K_2–Cu_1, and (c) Fe–Zn–K_2–Ru_1. (0.2 g sample; K/Fe = 0.02, Cu(Ru)/Fe = 0.01; 0.167 K/s ramping rate; 20% H_2/Ar, 0.268 mol/h flow rate).

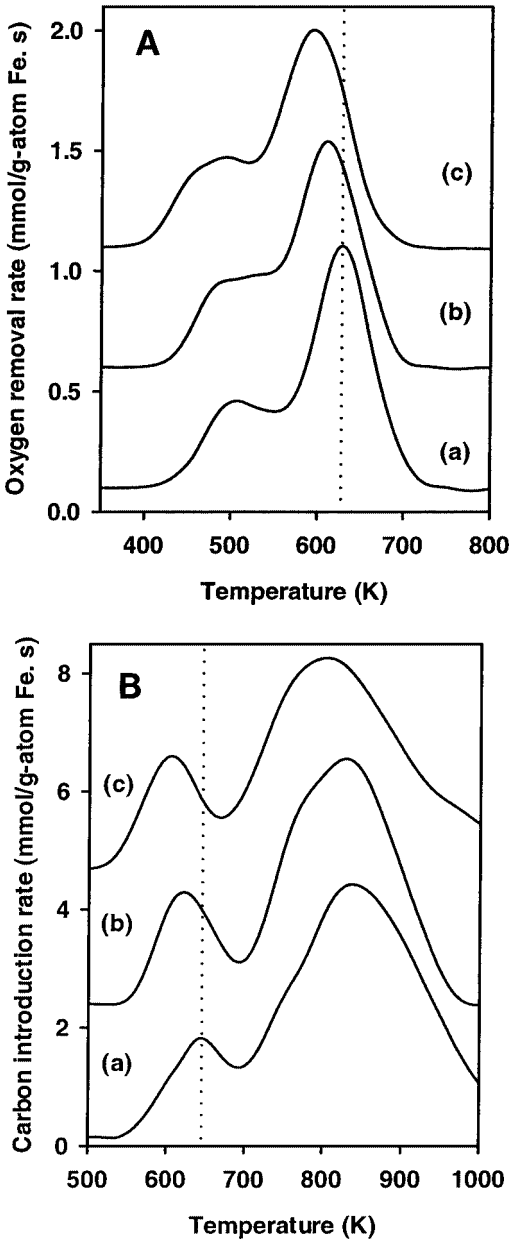

FIG. 2. (A) Oxygen removal and (B) carbon introduction rates for Fe–Zn–K–Cu(Ru) samples in CO. (a) Fe–Zn–K_2, (b) Fe–Zn–K_2–Cu_1, and (c) Fe–Zn–K_2–Ru_1. (0.05 g sample; K/Fe = 0.02, Cu(Ru)/Fe = 0.01; 0.167 K/s ramping rate; 20% CO/Ar, 0.268 mol/h flow rate).

dissociation rates than for oxide precursors promoted with similar numbers of Cu atoms.

Figure 2 shows oxygen removal and carbon introduction rates for Fe–Zn–K–Cu and Fe–Zn–K–Ru oxides as a function of temperature using CO as the reducing and carburizing reagent. Fe–Zn–K–Cu(Ru) oxides react with CO via reduction/carburization steps identical to those for pure Fe_2O_3 (5). Fe_2O_3 reacts with CO to form Fe_3O_4 and the latter simultaneously reduces and carburizes to form a mixture of $Fe_{2.5}C$ and Fe_3C, denoted here as FeC_x and confirmed by X-ray diffraction (5). The temperature required for these reduction–carburization steps is lowest for Fe–Zn–K_2–Ru_1 and highest for samples without Cu or Ru (Fe–Zn–K_2). Ru-promoted samples reduced and carburized at a temperature ~30 K lower than Cu-containing samples. The promoting effects of Ru and Cu on the reduction and carburization of Fe–Zn oxide precursors by CO were weaker than their respective effects when H_2 was used as the reductant, but Cu, and especially Ru, clearly increased the rate of oxygen removal when CO is used as the reductant. The effects of Ru and Cu on the rate of reduction and carburization of Fe–Zn oxides suggest that these components increase the initial rate of nucleation of reduced Fe-containing phases (Fe_3O_4, FeC_x). The resulting larger number of nuclei then leads to a better dispersion of these reduced phases, as shown earlier (4), and to a larger number of active sites for Fischer–Tropsch synthesis reactions. This expectation was confirmed by the catalytic measurements reported in the next section.

Effect of Ru and Cu on Fischer–Tropsch Synthesis Rate and Selectivity

Fischer–Tropsch synthesis rates were measured on Fe–Zn–K_2, Fe–Zn–K_2–Cu_1, and Fe–Zn–K_2–Ru_1 samples at 508 K and 2.14 MPa. Measurements were conducted at different CO space velocities; steady-state hydrocarbon formation rates (mol CO/h.g-at.Fe) are shown in Fig. 3a as a function of the CO conversion level. These rates were higher on the Ru-promoted sample (Fe–Zn–K_2–Ru_1) than on Cu-promoted (Fe–Zn–K_2–Cu_1) or unpromoted (Fe–Zn–K_2) catalysts. The effects of increasing conversion on FTS rates were similar on all samples, suggesting that kinetic dependencies on reactant and product concentrations were similar on all catalysts. Ru and Cu appear to increase the number of active sites available on catalysts derived from Fe–Zn oxide precursors, without any detectable changes in CO conversion turnover rates, in the kinetics of chain growth or CO hydrogenation on active sites, or in the pathways available for these reactions. This is consistent with the nearly identical selectivities to C_{5+} (Fig. 3c) and CH_4 (compared in Table 1 at similar CO conversions), and with the similar α-olefin/n-paraffin ratios (Fig. 3d) among all catalysts at all conversion levels.

CO_2 selectivities increased with CO conversion on all three catalysts (Fig. 3b). They were higher on Cu- or Ru-promoted Fe–Zn–K oxides than on unpromoted catalysts at all conversion levels. The slopes of the CO_2 selectivity-CO conversion curves in Fig. 3b are similar on all three catalysts, suggesting that the rate of secondary water-gas shift reactions were not influenced by these promoters, even though high water-gas shift rates have been reported on Cu-based catalysts (7). The extrapolated y-intercepts in Fig. 3b reflect the relative rates of removal of chemisorbed oxygen atoms (formed in CO dissociation steps) using CO. Cu and Ru

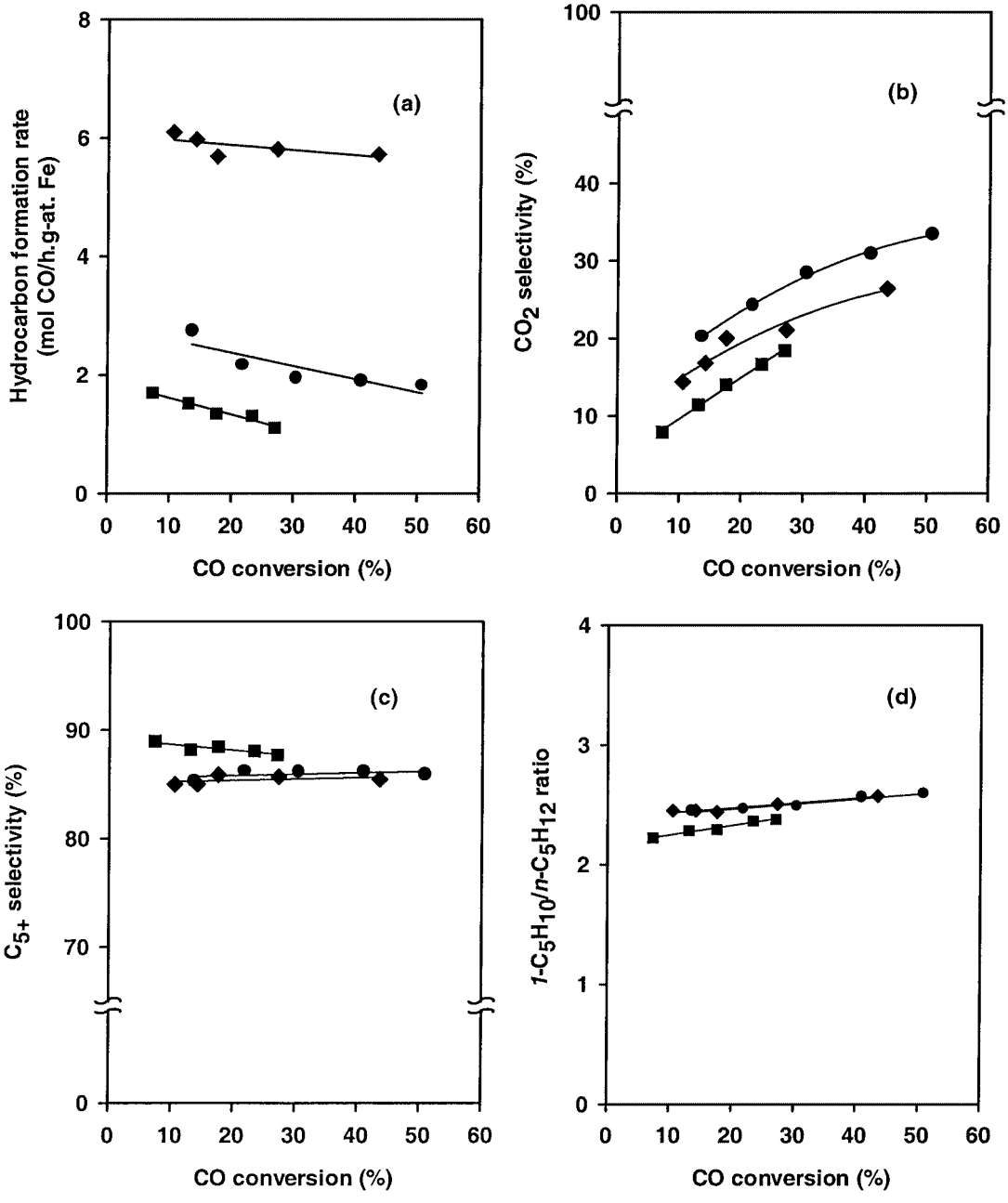

FIG. 3. Steady state FTS rates and selectivities on promoted Fe oxide catalysts as a function of CO conversion ($H_2/CO = 2$, 508 K and 2.14 MPa). (a) Hydrocarbon formation rate, (b) CO_2 selectivity, (c) C_{5+} selectivity, and (d) $1\text{-}C_5H_{10}/n\text{-}C_5/H_{12}$ ratio. Symbols: Fe–Zn–K_2 (squares), Fe–Zn–K_2–Cu_1 (circles), and Fe–Zn–K_2–Ru_1 (diamonds).

increase slightly the value of this intercept in Fig. 3b, suggesting an increase in the probability of oxygen removal via reactions with CO when these promoters are present. Another possible explanation for these higher intercepts is the presence of intrapellet H_2O concentration gradients caused by diffusional restrictions, which can become more severe within liquid-filled pores at the higher volumetric productivities typical of catalysts promoted with Cu or Ru.

The catalytic properties of Fe–Zn–K_2, Fe–Zn–K_2–Cu_1, and Fe–Zn–K_2–Ru_1 are compared at similar CO conversions in Table 1. The addition of Cu or Ru to Fe–Zn oxide precursors led to twofold and fourfold increases in hydrocarbon synthesis rates, respectively. These promotion effects cannot be explained by the FTS activity of the Ru promoter itself, which even if atomically dispersed, would account for less than 20% of the rate increase observed upon Ru addition, based on reported FTS turnover rates

TABLE 1

Steady State Fischer–Tropsch Synthesis Rates and Selectivities on Fe–Zn–K_2, Fe–Zn–K_2–Cu_1, and Fe–Zn–K_2–Ru_1 Samples

Sample	Fe–Zn–K_2	Fe–Zn–K_2–Cu_1	Fe–Zn–K_2–Cu_1
CO conversion rate (mol Co/h.g-at. Fe)	1.7	3.5	7.2
CO_2 formation rate (mol CO/h.g-at. Fe)	0.2	0.7	1.1
Hydrocarbon formation rate (mol CO/h.g-at.Fe)	1.5	2.8	6.0
CO_2 selectivity (%)	11.5	20.2	16.8
CH_4 selectivity (%)[a]	2.0	2.4	2.8
C_{5+} selectivity (%)[a]	88.2	85.3	85.0
1-C_5H_{10}/*n*-C_5H_{12} ratio	2.3	2.5	2.5

Note. Atomic ratios: Zn/Fe = 0.1, K/Fe = 0.02, Cu(Ru)/Fe = 0.01; $H_2/CO = 2$, 508 K, 2.14 MPa, CO conversion is 13–16%.

[a] CH_4 and C_{5+} selectivities are reported on a CO_2-free basis.

on Ru (20). C_{5+} formation rates increased proportionately with the observed increase in hydrocarbon synthesis rates, leading to nearly identical C_{5+} selectivities on all catalysts. The slightly lighter products formed on samples promoted with Cu or Ru reflect the lower surface density of the potassium promoter at the higher surface areas prevalent in metal-promoted samples, as discussed below. Ru, and to a lesser extent Cu, appear to increase the number of FTS active sites formed during the activation of Fe–Zn oxide precursors. This proposal is confirmed below by measurements of the structural evolution of the active phases during reaction and of the surface area and CO chemisorption uptakes after catalyst activation and Fischer–Tropsch synthesis reactions.

Surface Areas and CO Chemisorption Site Densities on Fresh and Activated Fe–Zn–K–Cu(Ru) Oxides

Table 2 shows BET surface areas and CO chemisorption uptakes on Fe–Zn–K_2, Fe–Zn–K_2–Cu_1, and Fe–Zn–K_2–Ru_1 oxide precursors after FTS reactions for 1 h at the conditions indicated. BET surface areas are also reported for the oxide precursors after thermal treatment in air at 673 K for 4 h, but before FTS reactions. Before reaction, BET surface areas were not affected by the presence of Cu or Ru promoters. After FTS reactions for 1 h, surface areas were higher on the metal-promoted samples than on unpromoted samples, suggesting that activation steps lead to smaller Fe_3O_4 and FeC_x crystallites when Cu or Ru are present during *in situ* treatment of Fe–Zn oxide precursors in synthesis gas.

CO chemisorption uptakes on activated samples were much higher when Cu or Ru were present, suggesting also the presence of a larger number of CO adsorption sites when Fe–Zn oxide precursors are activated in the presence of Cu or Ru. Chemisorption uptakes were higher on the Ru-promoted sample than on the Cu-promoted sample, a trend also observed for hydrocarbon synthesis rates. This parallel increase in FTS rates and CO chemisorption uptakes was also observed on Zn-free Fe–K–Cu samples (4). It is consistent with a role of Cu and Ru in the formation of smaller Fe carbide crystallites, which in turn provide a higher density of sites for CO chemisorption and for FTS reaction turnovers. Thus, it appears that these reduction–carburization promoters increase the rate of catalyst activation by providing a large number of nucleation sites, which favor the formation of smaller FeC_x and Fe_3O_4 crystallites. These smaller crystallites, and the faster carburization kinetics introduced by Cu and Ru, were probed directly

TABLE 2

BET Surface Areas and CO Chemisorption Uptakes on Fe–Zn–K_2, Fe–Zn–K_2–Cu_1, and Fe–Zn–K_2–Ru_1 Samples after FTS Reactions ($H_2/CO = 2$, 523 K, 1 h)

Sample	Fe–Zn–K_2	Fe–Zn–K_2–Cu_1	Fe–Zn–K_2–Ru_1
Surface area before FTS (m^2/g)	56	65	63
Surface area after FTS[a] (m^2/g)	23	31	39
Amount of CO_x desorbed before CO chemisorption (mmol/g-at. Fe)	11.3	65.3	68.4
Amount of CO_x desorbed after CO chemisorption (mmol/g-at. Fe)	31.6	109.9	124.5
Amount of CO chemisorbed (mmol CO/g-at. Fe)	20.3	44.6	58.1
FeC_x concentration[b] (atom%)	11.8	23.6	57.1
CH_4 formation rate[c] (mmol/s.g-at.Fe)	0.173	0.262	0.372

Note. Fe carbide concentrations were obtained from *in situ* XAS measurements; CH_4 formation rates were obtained from isothermal transient experiments.

[a] Surface areas measured after exposure to synthesis gas at 523 K for 1 h (0.2 g sample, K/Fe = 0.02, Cu/Fe = 0.01, $H_2/CO = 2$, synthesis gas flow rate = 64.3 mol/h.g-at. Fe).

[b] FeC_x concentration measured after exposure to synthesis gas at 523 K for 5 h (1 mg precipitated Fe_2O_3, K/Fe = 0.02, Cu/Fe = 0.01, $H_2/CO = 2$, synthesis gas flow rate = 107 mol/h.g-at. Fe).

[c] CH_4 formation rates measured after exposure to synthesis gas at 523 K for 1 h (0.2 g sample, K/Fe = 0.02, Cu/Fe = 0.01, $H_2/CO = 2$, synthesis gas flow rate = 64.3 mol/h.g-at. Fe).

during activation of Fe–Zn oxide precursors using *in situ* X-ray absorption spectroscopy, as described in the next section.

Structural Characterization of Fe–Zn–K–Cu(Ru) Catalysts During Fischer–Tropsch Synthesis Using X-Ray Absorption Spectroscopy

In situ Fe K-edge X-ray absorption spectroscopy was used to monitor the structural evolution of Fe–Zn oxides during activation and FTS reactions and the effects of Cu and Ru on the kinetics of formation and on the relative abundance of species formed as Fe–Zn oxide precursors undergo activation during contact with synthesis gas. Fe_2O_3, Fe_3O_4, and FeC_x were identified by principal component analysis and the sample spectra were described as linear combinations of these standard compounds as a function of time in contact with synthesis gas. FeC_x concentrations are reported as Fe atomic fractions as a function of contact time in Fig. 4. The reduction and carburization rates and the extent of carburization of these materials are smaller than those for the Zn-free samples reported previously (4), because Zn species, in the form of $ZnFe_2O_4$, inhibit reduction and carburization rates (5). The structure evolves, however, in a manner similar to that previously reported for Zn-free samples—via the initial formation of Fe_3O_4 and the rapid subsequent transformation of this phase into FeC_x (4). The details of such transformations are very similar for Fe and Fe–Zn oxide precursors; therefore, we restrict our discussion here to the extent and kinetics of FeC_x formation and to the effect of Cu and Ru on these properties for Fe–Zn oxide precursors.

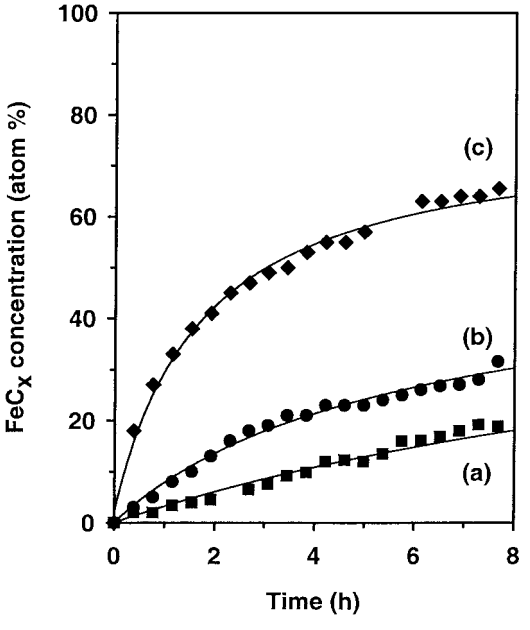

FIG. 4. The evolution of Fe carbides during *in situ* XAS measurement of Fe–Zn–K–Cu(Ru) samples in synthesis gas. (a) Fe–Zn–K_2, (b) Fe–Zn–K_2–Cu_1, and (c) Fe–Zn–K_2–Ru_1. (1 mg sample, K/Fe = 0.02, Cu(Ru)/Fe = 0.01, $H_2/CO = 2$, synthesis gas flow rate = 107 mol/h.g-at. Fe).

Figure 4 shows that Cu, and especially Ru, increased carburization rates and the steady-state extent of carburization of Fe–Zn oxide precursors promoted also with K. The faster carburization kinetics of these oxides in synthesis gas when promoted with Ru or Cu are similar to the faster reduction in H_2 or CO discussed above. As shown in Fig. 4, the extent of carburization is also higher on samples promoted with Ru or Cu than on the Fe–Zn–K sample. The FeC_x content, however, reached a nearly constant value after ~8 h on stream at the conditions of this study (Fig. 4). Thus, while faster carburization may lead to more rapid attainment of steady state FTS reaction rates, it should not lead to higher steady state FTS reaction rates, which are measured after contact with synthesis gas for more than 24 h. In addition, it is not obvious how the greater extent of carburization achieved when Cu or Ru are present would lead to higher steady state FTS rates, because previous studies using Fe_2O_3 precursors have shown that the carburization of one or two near-surface layers is sufficient to attain steady state FTS reaction rates (21). We conclude that the extent of carburization is controlled by the diffusion path for the removal of lattice oxygen from the core of Fe oxide precursors. Thus, the shorter diffusion path within the smaller crystallites formed during activation on promoted samples is responsible for the greater extent of carburization on the promoted samples. In this manner, both the higher FTS rates and the faster and more extensive carburization find a common cause in the role of promoters in nucleating Fe active phase as smaller crystallites. No causal relationship between the extent of carburization and the observed FTS reaction rates is warranted by these observations.

Isothermal Transient Analysis of Reduction, Carburization, and Fischer–Tropsch Synthesis Products during Activation of Fe–Zn–K–Cu(Ru) Catalysts

Fischer–Tropsch synthesis rates were measured during exposure to synthesis gas at the same conditions as those used to measure X-ray absorption spectra of these samples ($H_2/CO = 2$, 523 K). These studies aim to relate the observed structural evolution to the rate of hydrocarbon formation as Fe oxide catalyst precursors activate during FTS. CH_4 formation rates on Fe–Zn–K oxide precursors promoted with Cu or Ru are shown in Fig. 5 as a function of time on stream. For unpromoted Fe–Zn–K oxides, a short induction period was observed upon initial contact with synthesis gas. CH_4 was immediately detected, however, on Fe–Zn–K oxides promoted with Cu or Ru. CH_4 formation rates during initial contact with synthesis gas and at steady-state were higher on promoted catalysts than on unpromoted oxide precursors (Fig. 5). The initial increase in

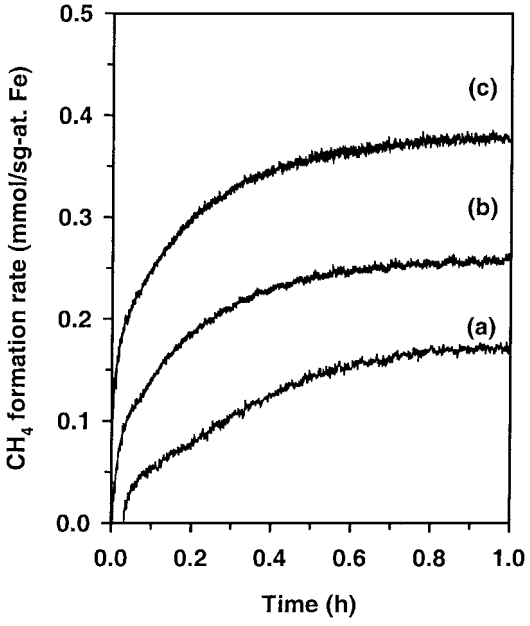

FIG. 5. CH_4 formation rate as a function of reaction time in contact with synthesis gas ($H_2/CO = 2$, 523 K, synthesis gas flow rate = 107 mol/h.g-at. Fe). (a) Fe–Zn–K_2, (b) Fe–Zn–K_2–Cu_1, and (c) Fe–Zn–K_2–Ru_1 samples.

CH_4 formation rates is accompanied by the formation of an excess amount of CO_2 and H_2O, indicative of the removal of lattice oxygen during the initial reduction and carburization of the oxide precursors. These reduction–carburization processes are faster on Ru-containing samples than on Cu-containing or unpromoted Fe–Zn–K samples. Steady state FTS rates were attained after ~1 h in contact with synthesis gas, even though X-ray absorption spectra detected a continuing increase in FeC_x content up to ~8 h. These data confirm the previous proposal that FTS reactions are influenced only by the density of reduced Fe centers in near-surface layers, irrespective of the presence of a remaining Fe oxide core (21). These data are also consistent with FTS data obtained at higher pressures and reported above, and with a role of Cu or Ru in nucleating smaller and more easily reduced and carburized structures from Fe–Zn–K oxide precursors.

On samples containing Cu or Ru (Table 2), FTS rates increased proportionally with the observed increase in FeC_x content and in CO chemisorption uptakes. All these results clearly show that Cu and Ru favor the formation of a more dispersed active phase, and that chemical promotion effects, such as an increase in the turnover rate of FeC_x sites, are unnecessary in order to account for the observed increase in FTS rates when Cu or Ru are present during the activation of Fe–Zn oxide precursors. These conclusions, taken together with the previous observation that higher surface area precursors prepared by incorporating ZnO during the precipitation of Fe_2O_3 also led to higher FTS reaction rates (6), led us to attempt the synthesis of more highly dispersed active structures by using Fe oxide precursors with higher surface areas.

Synthesis of Fe–Zn–K–Cu Oxide Precursors with Higher Surface Areas

Our efforts to improve the dispersion and site density of the active structures formed during reaction included the use of promoters and synthesis procedures in order to increase the surface area of Fe–Zn oxide precursors and to minimize the sintering that occurs during drying and impregnation with Cu(Ru) and K. In this section, we examine the promoter concentrations required in order to optimize catalysts prepared from precursors with varying surface areas. We also show that the surface density of the Cu and K promoters (~2 K/nm^2 and 1 Cu/nm^2), and not their atomic content, are the relevant controlling variables in determining the dispersion and catalytic properties of FeC_x structures.

Several factors, such as the drying processes after precipitation or impregnation and the temperature and time of thermal treatments designed to decompose precursors, influence the surface area of Fe–Zn oxide precursors. These factors were systematically examined in order to increase catalyst surface areas and FTS reaction rates. The effect of precipitation pH was examined previously; it was found that a pH of 7.0 held constant during precipitation, led to the highest precursor surface areas (22). The effect of Zn/Fe ratio on the performance of Fe–Zn–K catalysts for FTS reactions was also previously examined and a Zn/Fe atomic ratio of 0.1 was found to give highest FTS reaction rates (23).

Sintering of porous materials often occurs as a result of pore mouth pinching during the final stages of evaporation of intrapore liquids with high surface tension, even at low temperatures. This process is particularly severe during evaporation of aqueous phases, because of their high surface tension ($\gamma = 72$ mN/m at 298 K). Alcohols have lower surface tensions (22 mN/m for ethanol and isopropanol); they also act as surface-active agents that decrease the surface tension of aqueous solutions (11). Therefore, most of the water contained within the pores in Fe–Zn oxide precipitates was replaced by extensive washing with either ethanol or isopropanol before drying in an attempt to inhibit sintering of Fe–Zn oxide precursors during evaporation of intrapore liquids.

Figure 6 shows the surface area of Fe–Zn oxide precursors containing various intrapore liquids after thermal treatment at various temperatures (Figs. 6a–6c). After drying at 398 K for 12 h, precipitates washed with ethanol or isopropanol showed higher Fe–Zn oxyhydroxide surface areas than precipitates dried without replacing any of the intrapore water with alcohols (215 vs 148 m^2/g). The similar precursor surface areas obtained with isopropanol and ethanol are consistent with the similar surface tension

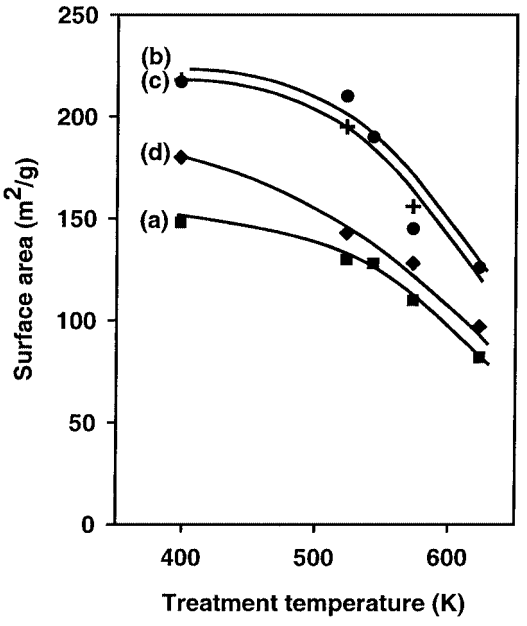

FIG. 6. BET surface areas of Fe–Zn and Fe–Zn–K_2–Ru_1 samples dried with various intrapore liquids as a function of thermal treatment temperature. (a) Fe–Zn precursor washed by intrapore water (squares), (b) Fe–Zn precursor washed by intrapore ethanol (circles), (c) Fe–Zn precursor washed by intrapore isopropanol (+), (d) Fe–Zn precursor washed by ethanol and subsequently promoted with K and Ru (diamonds) (K/Fe = 0.02, Ru/Fe = 0.01). (All the samples were treated in dry air at the stated temperature for 4 h).

of these two liquids. All other precipitation variables were kept constant; therefore, it appears that the drying step and the surface tension of the intrapore liquids during drying strongly influenced the pore structure and the surface area of the Fe–Zn oxide precursors. Our data show that a high space velocity of dry air (~2000 cm^3/h.g-cat.) is also required in order to minimize sintering during the decomposition of these oxyhydroxide precursors. A decrease in the surface tension of intrapellet liquids and the rapid removal of H_2O during oxyhydroxide decomposition are essential in preserving the high surface area of the oxide precursors.

The temperature and time of the final thermal treatment in air also influenced Fe–Zn oxide surface areas. After drying oxyhydroxide precipitates with different intrapore liquids at 398 K for 12 h, they were treated in flowing dry air at various temperatures for 4 h in order to determine optimum treatment protocols. All samples showed the decrease in surface area expected with increasing treatment temperature, but the higher surface area samples obtained by drying alcohol-containing precipitates were more sensitive to the thermal treatment temperature. X-ray diffraction confirmed that Fe–Zn hydroxides convert to poorly crystalline Fe_2O_3 at ~543 K. Zn, possibly as the $ZnFe_2O_4$ phase detected in samples with higher Zn/Fe ratios (>0.2) and treated at higher temperatures (~673 K), was well dispersed and not detected in these alcohol-washed samples. It appears that thermal treatment at 543 K provides a compromise between structural purity and a high surface area in Fe_2O_3, and that the surface area of the resulting oxide is highest when intrapore water is replaced with lower surface tension liquids, such as alcohols.

The effects of impregnation with K and Cu promoters on surface areas were also investigated. Fe–Zn oxyhydroxide precursors were impregnated with K carbonate (K/Fe = 0.02) and dried at 393 K for 12 h. Ru (Ru/Fe = 0.01) was then added as Ru nitrosyl nitrate using similar impregnation procedures. The addition of K to Fe–Zn hydroxide precursors decreased its surface area (220 vs 192 m^2/g), apparently because of pore collapse caused by the removal of high surface tension intrapore liquids. Similarly, the subsequent impregnation of Fe–Zn–K with Ru led to an additional decrease in its surface area. Each impregnation and subsequent drying decreased the surface area by 10–20%. Ru-promoted Fe–Zn–K hydroxides were then treated at different temperatures in order to examine the effect of treatment temperature on surface area (Fig. 4d). The effects of temperature on the surface area of Fe–Zn–K–Ru oxides were similar to those found in Fe–Zn oxides. The surface area of Ru-promoted Fe–Zn–K oxides decreased from 142 to 96 m^2/g as the thermal treatment temperature increased from 523 to 623 K.

Based on these surface areas for Fe–Zn hydroxides and Fe–Zn–K–Ru oxide precursors prepared by different methods, we selected a procedure for maximizing the surface area of Fe–Zn–K–Cu samples. Fe–Zn hydroxide precursors were first prepared by coprecipitation at a constant pH of 7.0 and the precipitates were thoroughly washed with ethanol in order to replace intrapore water. Fe–Zn hydroxide precursors were then treated at 543 K for 4 h in flowing dry air (2000 cm^3/h.g-cat). The resulting Fe–Zn oxide precursors were impregnated with K and Cu using incipient wetness impregnation method and aqueous solutions of Cu nitrate and K carbonate. The amounts of K (K/Fe = 0.04) and Cu (Cu/Fe = 0.02) were chosen so as to maintain the K and Cu surface densities at the levels previously shown to lead to maximum FTS reaction rates on conventionally prepared samples (~2 K-atom/nm^2; 1 Cu-atom/nm^2) (6). The surface area of the resulting Fe–Zn–K_4–Cu_2 oxides was 120 m^2/g, almost twice that of the Fe–Zn–K_2–Cu_1 oxide samples. As a result, the K and Cu content were chosen to be about twice as high as those in the conventionally prepared Fe–Zn–K_2–Cu_1 sample. A Fe–Zn–K_2–Cu_1 sample prepared from high surface area Fe–Zn oxide precursors led to lower FTS rates and to significantly lighter products than a sample with the higher promoter concentrations (Fe–Zn–K_4–Cu_2), suggesting the presence of suboptimum levels of K and Cu and confirming the relevant role of atomic surface density as the defining variable in the design of these promoted catalytic materials.

Site Density of Active Species and Promoters and Its Effects on Fischer–Tropsch Synthesis Rate and Selectivity

The relevance of improvements in surface area to the performance of these materials in FTS reactions was confirmed by measuring FTS rates and selectivities on a high surface area Fe–Zn–K_4–Cu_2 oxide (120 m^2/g) prepared by the method described in the previous section and on a lower surface area Fe–Zn–K_2–Cu_1 oxide prepared via conventional methods (65 m^2/g). The amounts of K and Cu in the Fe–Zn–K_4–Cu_2 sample were chosen in order to maintain the same surface density of promoters as in the Fe–Zn–K_2–Cu_1 sample prepared from Fe–Zn oxide precursors with lower surface area. Steady-state FTS rates and selectivities at 508 K and 2.14 MPa are shown as a function of CO conversion in Fig. 7. Hydrocarbon synthesis rates are about twofold higher on Fe–Zn–K_4–Cu_2 than on Fe–Zn–K_2–Cu_1, a difference that parallels the difference in surface area between their respective Fe–Zn oxide precursors. The similarities between these two samples in CO_2 and C_{5+}

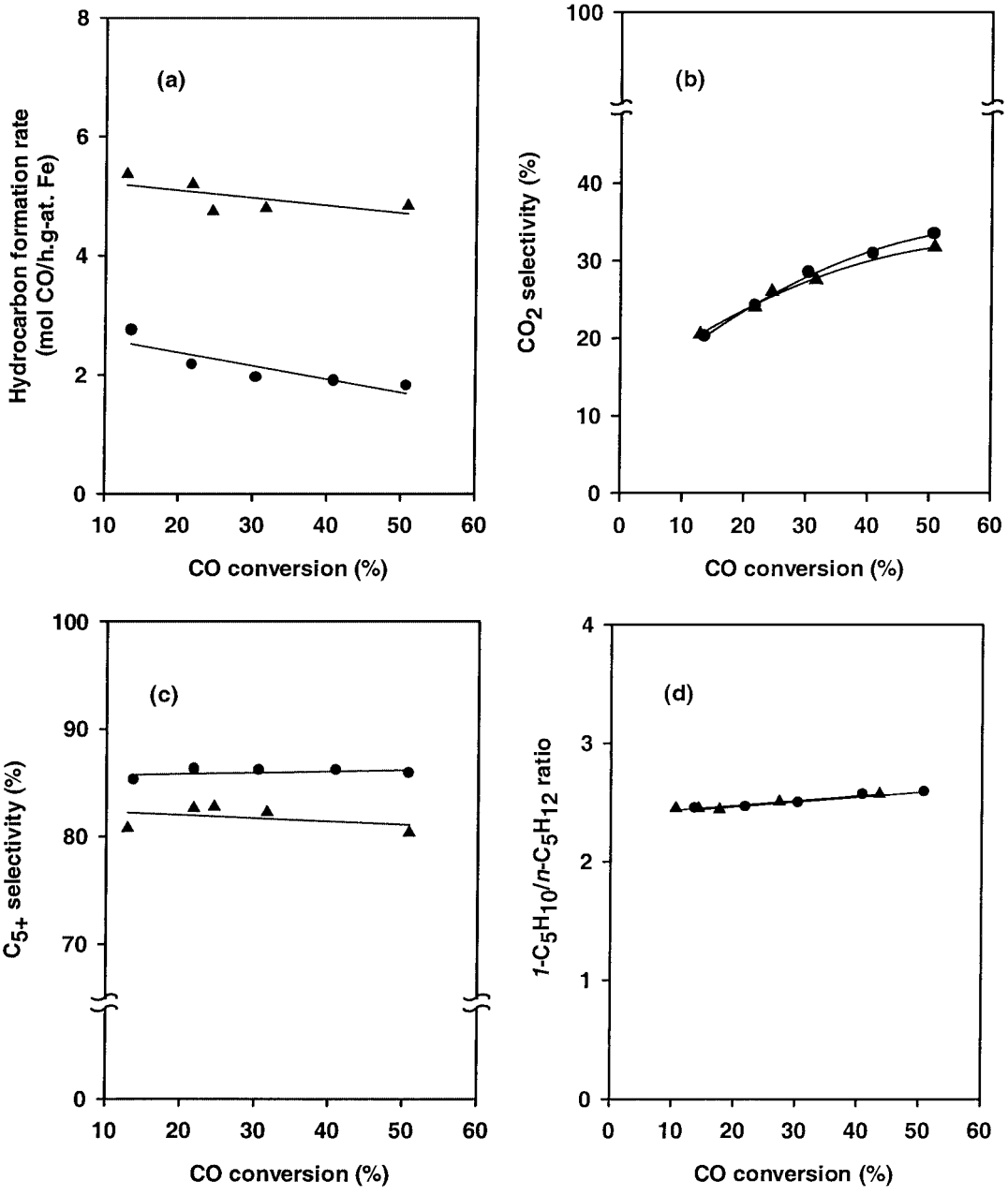

FIG. 7. Comparison of the FTS performance of Fe–Zn–K_2–Cu_1 (circle) and Fe–Zn–K_4–Cu_2 (triangle) samples as a function of CO conversion at steady-state reaction conditions ($H_2/CO = 2$, 508 K and 2.14 MPa). (a) Hydrocarbon formation rate, (b) CO_2 selectivity, (c) C_{5+} selectivity, and (d) $1\text{-}C_5H_{10}/n\text{-}C_5/H_{12}$ ratio.

selectivities, in α-olefin/n-paraffin ratios, and in their kinetic response of FTS rates to changes in conversion, suggest that the synthetic protocols used to increase the precursor surface areas led to a larger number of active sites in working catalysts, without any detectable changes in chain growth pathways.

Figure 8 shows FeC_x concentrations obtained from XAS measurements of the structural evolution of these oxide precursors during FTS reactions. Figure 9 shows the corresponding CH_4 formation rates on these two samples at the same conditions used in X-ray absorption experiments. Both the extent of carbide formation and the steady-state CH_4 formation rate were significantly higher on Fe–Zn–K_4–Cu_2 than on Fe–Zn–K_2–Cu_1 samples. The consistent correlation between the Fe carbide concentration and FTS rates is again not causal. It confirms that promoters (Ru, Cu, K) and higher surface area precursors increase the density of active sites in the reduced active structures prevalent during steady-state Fischer–Tropsch synthesis. Accordingly, we examined next whether further increases in the surface density of these promoters would lead to additional improvements in their active site density and FTS rates. We prepared a Fe–Zn–K–Cu sample using the same Fe–Zn oxide precursor and treated the sample at the same conditions as the Fe–Zn–K_2–Cu_1 sample but added a higher K concentration (Fe–Zn–K_4–Cu_1).

Table 3 compares FTS performance, surface area, CO chemisorption uptake, and the extent of carburization for Fe–Zn–K_2–Cu_1, Fe–Zn–K_4–Cu_1, and Fe–Zn–K_4–Cu_2 catalysts. Fe–Zn–K_2–Cu_1 and Fe–Zn–K_4–Cu_1 samples have similar surface areas but different potassium contents and surface densities (2 vs 4 K/nm^2); yet, similar FTS reaction rates, CO chemisorption uptakes, and extents of carburization were obtained. This suggests that the higher K surface density did not lead to a further increase in the number of active sites, possibly because excess potassium leads to larger domains of the promoter without significantly better contact between the promoter and the Fe oxide precursors or to a higher actual surface density of potassium carbonate species. We have observed that increasing Cu or K concentrations beyond those required to achieve surface densities of 1 and 2 atom/nm^2, respectively, does not increase FTS reaction rates on conventionally prepared samples. Fe–Zn–K_2–Cu_1 and Fe–Zn–K_4–Cu_2 samples have different BET surface areas but similar apparent surface densities of K and Cu on the available surface area. The Fe–Zn–K_4–Cu_2 sample with the higher surface area shows higher FTS rates and higher densities of CO binding sites, indicating that higher precursor surface areas lead to proportionately higher FTS rates and active site densities, as long as the promoter surface densities are kept above a threshold level. These results suggest that promoter concentrations are more appropriately defined in terms of surface density in designing catalysts with similar and optimum promoter contents as the surface area of Fe oxide precursors are changed by modifying precipitation, drying, and promoter impregnation methods. The parallel observed increases in FTS rates, surface area, CO adsorption site density, and steady-state

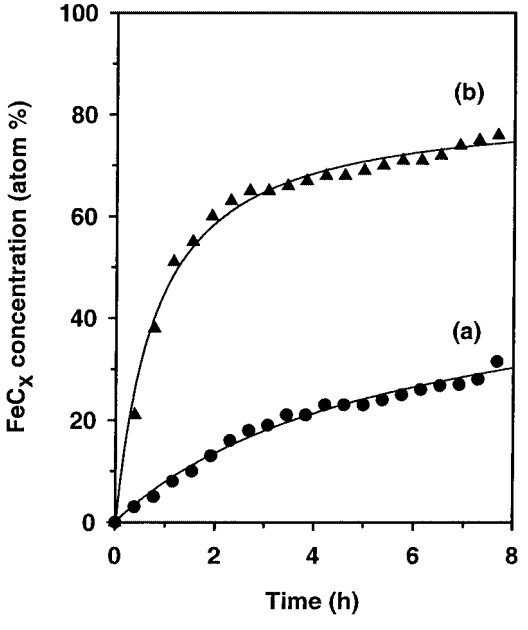

FIG. 8. FeC_x concentrations as a function of time on (a) Fe–Zn–K_2–Cu_1 and (b) Fe–Zn–K_4–Cu_2 samples as a function of reaction time during *in situ* X-ray absorption measurements in synthesis gas (1 mg precipitated sample, $H_2/CO = 2$, synthesis gas flow rate = 107 mol/h.g-at. Fe).

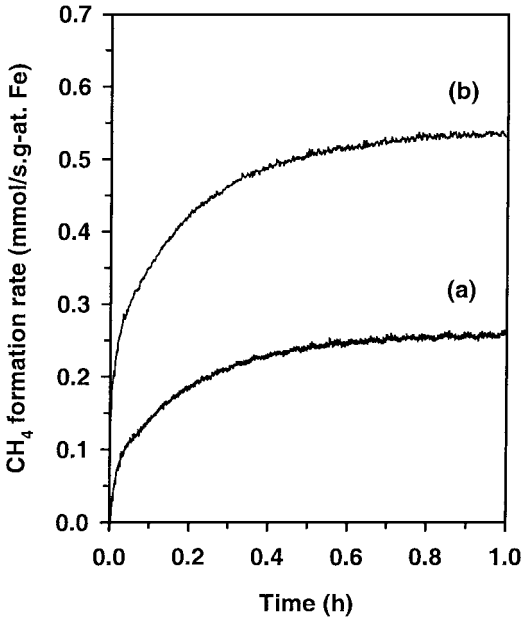

FIG. 9. CH_4 formation rates as a function of time in contact with synthesis gas at the conditions of X-ray absorption measurements shown in Fig. 8 ($H_2/CO = 2$, 523 K, synthesis gas flow rate = 107 mol/h.g-at. Fe). (a) Fe–Zn–K_2–Cu_1 sample, (b) Fe–Zn–K_4–Cu_2 sample.

TABLE 3

Steady State FTS Rates and Selectivities ($H_2/CO = 2$, 508 K, 2.14 MPa, CO conversion is 13–16%) and the Characterization Results for Fe–Zn–K_2–Cu_1, Fe–Zn–K_4–Cu_1, and Fe–Zn–K_4–Cu_2 Samples after FTS Reactions

Sample	Fe–Zn–K_2–Cu_1	Fe–Zn–K_4–Cu_1	Fe–Zn–K_4–Cu_2
CO conversion rate (mol CO/h.g-at. Fe)	3.5	3.6	6.8
CO_2 formation rate (mol CO/h.g-at. Fe)	0.7	0.8	1.4
Hydrocarbon formation rate (mol CO/h.g-at. Fe)	2.8	2.8	5.4
CO_2 selectivity (%)	20.2	22.4	20.5
CH_4 selectivity (%)[a]	2.4	2.4	3.8
C_{5+} selectivity (%)[a]	85.3	85.5	80.8
1-C_5H_{10}/*n*-C_5H_{12} ratio	2.5	2.5	2.7
Surface area before FTS (m^2/g)	65	58	120
Surface area after FTS[b] (m^2/g)	31	26	43
Amount of CO_x desorbed before CO chemisorption (mmol/g-at. Fe)	65.3	72.0	75.2
Amount of CO_x desorbed after CO chemisorption (mmol/g-at. Fe)	109.9	112.3	141.1
Amount of CO chemisorbed (mmol CO/g-at. Fe)	44.6	40.3	65.9
FeC_x concentration[c] (atom %)	23.6	—	69.2
CH_4 formation rate[d] (mmol/s.g-at. Fe)	0.262	0.289	0.527

[a] CH_4 and C_{5+} selectivities are reported on a CO_2-free basis.

[b] Surface areas measured after exposure to synthesis gas at 523 K for 1 h (0.2 g sample, K/Fe = 0.02, Cu/Fe = 0.01, $H_2/CO = 2$, synthesis gas flow rate = 64.3 mol/h.g-at. Fe).

[c] FeC_x concentration measured after exposure to synthesis gas at 523 K for 5 h (1 mg precipitated Fe_2O_3, K/Fe = 0.02, Cu/Fe = 0.01, $H_2/CO = 2$, synthesis gas flow rate = 107 mol/h g-at. Fe).

[d] CH_4 formation rates measured after exposure to synthesis gas at 523 K from 1 h (0.2 g sample, K/Fe = 0.02, Cu/Fe = 0.01, $H_2/CO = 2$, synthesis gas flow rate = 64.3 mol/h.g-at. Fe).

concentration of Fe carbide suggest that higher FTS activity can be achieved by the design and appropriate promotion of high surface area oxide precursors.

Fischer–Tropsch Synthesis Rates and Selectivities on Fe–Zn–K_4–Cu_2 and Co-Based Catalysts

The apparent low Fischer–Tropsch synthesis rates on Fe-based catalysts at reaction conditions typically used for Co-based catalysts (473–488 K) has led to their predominant use at higher temperatures (500–543 K). Here, we compare FTS reaction rates and selectivities on a Fe–Zn–K_4–Cu_2 catalyst with those on previously reported Fe-based catalysts. Also, we find that high surface area Fe–Zn–K_4–Cu_2 catalysts show hydrocarbon synthesis productivities similar to those observed on Co-based catalysts at conditions typically used for the latter (473 K, 2 MPa, $H_2/CO = 2$).

A Fe–Zn–K_4–Cu_2 sample is compared with the most active reported Fe-based catalysts in Table 4 for nearly stoichiometric reactants ($H_2/CO = 1.7$-2.0) and at relatively high CO conversions (~50%). The results from the low-surface area Fe–Zn–K_2–Cu_1 are representative of the catalyst reported in Ref. (6) sample. CO conversion rates and hydrocarbon synthesis productivities on Fe–Zn–K_4–Cu_2 are about twice those reported on the Ruhrchemie AG catalyst (Fe–SiO_2–$K_{5.9}$–$Cu_{4.4}$) (24), and nearly three times higher than for the Fe–Zn–K_2–Cu_1 catalyst, even though Fe–Zn–K_4–Cu_2 was tested at lower temperatures (508 K vs

TABLE 4

Steady State FTS Performance of Various Fe-Based Catalysts Using Natural Gas-Derived Synthesis Gas ($H_2/CO = 1.7$–2.0)

Catalyst	Fe–Zn–K_4–Cu_2 (this work)	Fe–Zn–K_2–Cu_1 (this work)	Fe–$Si_{4.6}$–$K_{1.4}$ (25, 26)	Fe–SiO_2–$K_{5.9}$–$Cu_{4.4}$ [Ruhrchemie LP33/81] (24)
Reactor type	Fixed-bed	Slurry	Slurry	Spinning basket
Temperature (K)	508	543	543	523
Pressure (MPa)	2.14	0.50	1.31	2.40
H_2/CO ratio	2.0	2.0	1.7	2.0
CO space velocity (NL/h.g-cat.)	3.4	1.4	5.7	2.4*
CO conversion (%)	50.8	55.5	50.0*	52.7
CO rate (mol CO/h.g-cat)	0.08	0.03	0.12*	0.05*
Hydrocarbon productivity (g/h.kg-cat.)	765	258	1008*	404
CO_2 selectivity (%)	31.7	48.6	40.0*	42.3*

* Values calculated based on reported data or graphs.

TABLE 5

A Comparison of the Steady-State FTS Rates and Selectivities on Fe and Co Catalysts (473 K, 2.0 MPa, $H_2/CO = 2$) at CO Conversion Range of 18∼21%

Catalyst	Fe–Zn–K_4–Cu_2	Co/SiO_2	Co-Re/TiO_2[a]
"Active" Sites Density for FTS ($\times 10^{-4}$ mol/g-cat.)[b]	7.4	1.7	—
Hydrocarbon synthesis turnover rate (h^{-1})	16.7	59.6	—
Hydrocarbon synthesis productivity (g/h-kg-cat.)	171	143	220
Hydrocarbon synthesis volumetric productivity (g-hydrocarbons/L-catalyst-h)	188	61	220
CO_2 selectivity (%)	15.8	0.3	0.2
CH_4 (%)[c]	2.0	6.8	4.5
C_2-C_4 (%)[c]	8.9	6.4	—
C_{5+} (%)[c]	89.1	86.8	—
1-C_5H_{10}/*n*-C_5H_{12} ratio	2.1	2.0	—
1-$C_{10}H_{20}$/*n*-$C_{10}H_{22}$ ratio	1.6	0.3	—

Note. Atomic ratios: Zn/Fe = 0.1, K/Fe = 0.04, Cu/Fe = 0.02; 21.9 wt.% Co/SiO_2.

[a] Reference 27, 12 wt.% Co-0.5 wt.% Re/TiO_2, 44% CO conversion; 1 g cm^{-3} catalyst density assumed.

[b] From CO chemisorption after FTS followed by quenching for Fe; from H_2 chemisorption on a pre-reduced fresh catalyst for Co.

[c] CH_4 and C_{5+} selectivities are reported on a CO_2-free basis.

523–543 K). Fe–Zn–K_4–Cu_2 also compares well with a Fe–$Si_{4.6}$–$K_{1.4}$ catalyst tested at 543 K (25, 26). CO_2 selectivities are lower on Fe–Zn–K_4–Cu_2 than on the other catalysts, predominately because of the lower reaction temperatures made possible by the high FTS rates on this sample. The rigorous implementation synthesis, promotion, and activation protocols designed to increase the density of FTS active sites have led to additional improvements in hydrocarbon synthesis productivities, even after several decades of active research on Fe-based FTS catalysts.

The high surface area Fe–Zn–K_4–Cu_2 sample was also compared with a Co/SiO_2 catalyst at conditions typical of Co-based FTS catalysts (Table 5). Data for a patented Co–Re/TiO_2 catalyst, representative of state-of-the-art commercial catalysts, are also shown in Table 5 (27). Fe-based catalysts typically require higher temperatures, while Co-based catalysts must be operated within narrow ranges of temperature (473–500 K), pressure (∼2 MPa), and synthesis gas stoichiometry ($H_2/CO \sim 2$), because of their predominant methanation activity at higher temperatures, lower pressures, or higher H_2/CO ratios.

The hydrocarbon synthesis productivity, CH_4 selectivity, C_{5+} selectivity, and *1*-pentene/*n*-pentane and *1*-decene/*n*-decane ratios are shown as a function of CO conversion on Fe–Zn–K_4–Cu_2 and Co/SiO_2 in Figs. 10a–10e. Table 5 provides a summary of these comparisons at similar CO conversions (18–21%). Hydrocarbon synthesis productivities are very similar on these two catalysts (Table 5, Fig. 10a). Hydrocarbon synthesis turnover rates estimated from the number of sites available on Co/SiO_2 (using H_2 chemisorption before reaction) and on Fe–Zn–K_4–Cu_2 (using CO chemisorption after reaction) are higher on the Co-based catalyst [Co; 60.9 h^{-1}; Fe; 19.8 h^{-1}] (Table 5). FTS rates increased slightly with CO conversion on Co catalysts, because of a promoting effect of the water product formed in FTS reactions (10). CH_4 selectivities (Fig. 10b) were lower on Fe than on Co catalysts, but C_{5+} selectivities (Fig. 10c) were very similar on the two catalysts, because of higher C_2–C_4 olefin selectivities on Fe (Fe: 8.9%; Co: 8.4%). The *1*-pentene/*n*-pentane ratios are similar on the two catalysts (Fig. 10d and Table 5). Larger hydrocarbons are essentially paraffinic on Co catalysts, because of extensive readsorption and chain initiation by larger α-olefins formed in primary chain termination steps, as shown by the *1*-decene/*n*-decane ratios on Co than on Fe catalysts (Fig. 10e, Table 5).

The comparison with Co–Re/TiO_2 is restricted to those details reported in the relevant patent document. Hydrocarbon synthesis productivities (per mass) on Co–Re/TiO_2 are slightly higher than on Co/SiO_2, apparently as a result of a slightly higher Co site density and of the water rate enhancements at the higher conversions used in the Co–Re/TiO_2 patent. Volumetric and mass-based productivities are very similar on Co–Re/TiO_2 and Fe–Zn–K_4–Cu_2 samples at conditions typically used for Co-based catalysts. Reaction temperatures on Co-based catalysts are restricted to ∼500 K because of significant C_{5+} selectivity losses, while much higher temperatures and productivities are attainable on the Fe-based catalysts of this study (Table 4).

In summary, hydrocarbon synthesis rates (per g) on Fe–Zn–K_4–Cu_2 catalysts prepared via the synthesis, promotion, and activation protocols reported here are nearly identical to those observed on Co-based catalysts representative of the state-of-the-art. The lower apparent turnover rates on Fe-based catalysts are compensated by a larger density of active sites per gram of catalyst to yield similar hydrocarbon synthesis rates per mass or volume of catalyst. The higher bed density of Fe oxide precursors relative to Co/SiO_2 leads to much higher volumetric productivities on Fe–Zn–K_4–Cu_2 (0.188 g-hydrocarbons/cm^3-catalyst.h)

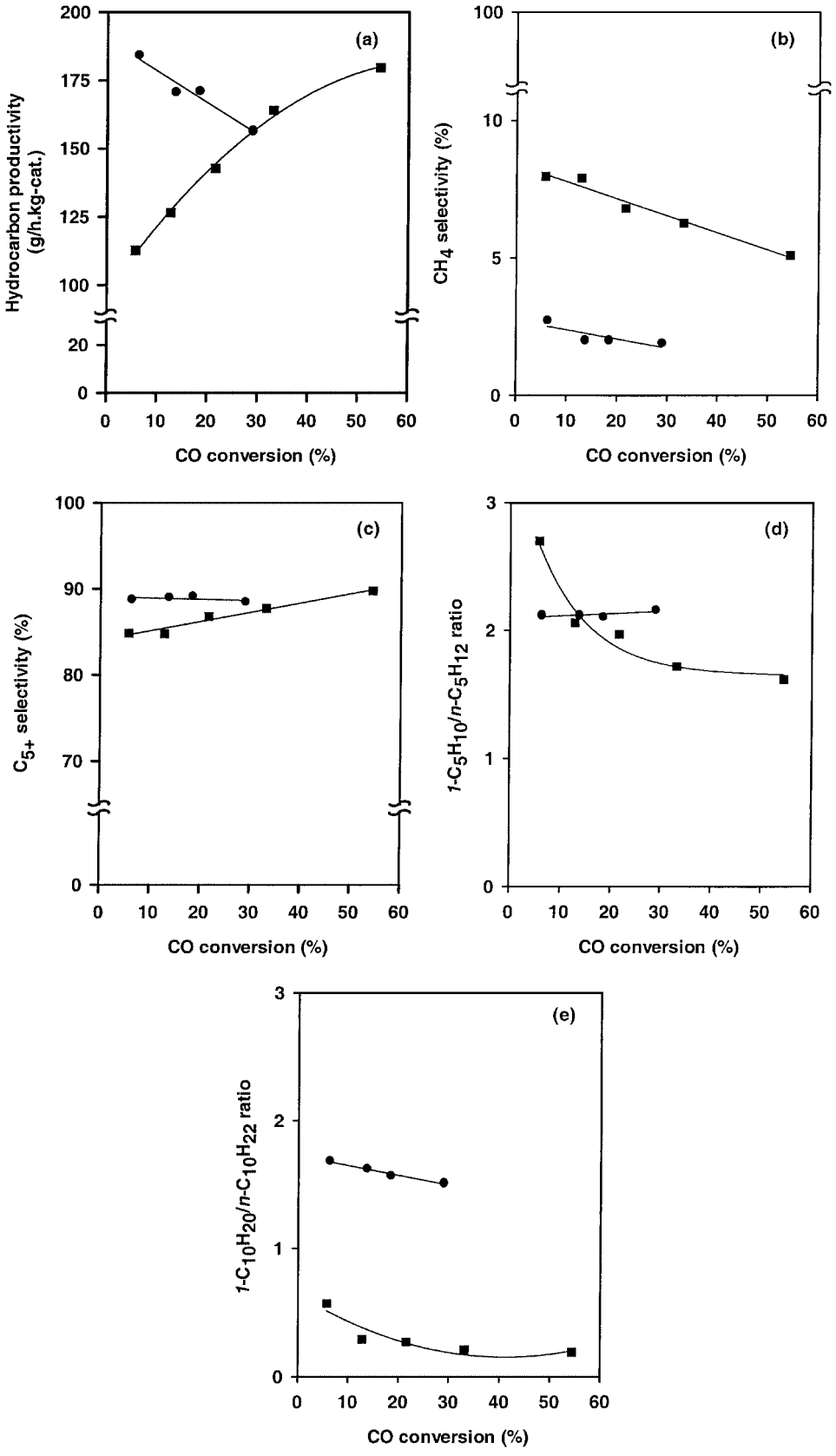

FIG. 10. Comparison of the performance of the Fe–Zn–K_4–Cu_2 (circles), and 21.9 wt% Co/SiO_2 (squares) catalysts for the FTS reactions (473 K and 2.14 MPa, $H_2/CO = 2$) (a) Hydrocarbon productivity, (b) CH_4 selectivity, (c) C_{5+} selectivity, (d) $1\text{-}C_5H_{10}/n\text{-}C_5H_{12}$ ratio, and (e) $1\text{-}C_{10}H_{20}/n\text{-}C_{10}/H_{22}$ ratio.

than on Co/SiO_2 (0.061 g-hydrocarbons/cm^3-catalyst.h), an advantage that can be used to decrease the reactor volumes required in packed bed or bubble column reactors. These Fe-based catalysts, with their lower CH_4 selectivities and more olefinic products, provide attractive alternatives to Co-based catalysts. These Fe-based catalysts also show a much weaker dependence of selectivity on temperature, pressure, and synthesis gas ratio than Co catalysts. Their higher CO_2 selectivity, even at low temperatures, continues to inhibit their use in the conversion of natural gas-derived synthesis gas. Additional decreases in CO_2 selectivities on Fe catalysts will require even lower reaction temperatures or the internal recycle of some CO_2 to the inlet of FTS or synthesis gas generation reactors.

CONCLUSIONS

The synthesis of high surface area precursors based on precipitated Fe–Zn oxides and their promotion with Cu, Ru, and K led to high Fischer–Tropsch synthesis rates and low CH_4 selectivities. These catalysts can be operated at mild conditions (473 K, 2.0 MPa) typically used for Co-based catalysts and they show similar hydrocarbon synthesis rates per catalysts mass or volume than representative Co-based FTS catalysts. The low reaction temperatures made possible by the high FTS activity of these Fe-based catalysts led to lower CO_2 than on Fe-based catalysts reported previously.

The presence of Cu or Ru in Fe–Zn–K oxide precursors led to higher reduction and carburization rates by activating H_2 and CO reactants and promoting the nucleation of reduced Fe species (Fe_3O_4, FeC_x) during the initial contact of the oxide precursors with synthesis gas. The resulting smaller crystallites of reduced Fe species lead to higher steady-state FTS rates than on unpromoted samples, and to a larger number of CO binding sites on steady state catalysts, without changes in product selectivity. They also lead to shorter diffusion distances during the interconversion of oxide and carbides in the presence of synthesis gas and to a greater extent of carburization during FTS reactions.

Higher FTS reaction rates were also achieved by increasing the surface area of Fe–Zn oxide precursors, which led to a corresponding increase in the number of CO binding sites available during reaction. The replacement of intrapore liquid water with lower surface tension alcohols inhibited the loss of precursor surface area by pore closure during drying. A study of the effects of promoter content on rates and selectivities for Fe–Zn oxide precursors showed that the promoter surface density was the relevant variable in determining the effectiveness of these promoters, at least up to threshold values of 1 Cu/nm^2 and 2 K/nm^2. Thus, high surface area oxides were promoted with a proportionately larger amount of Cu (or Ru) and K so as to maintain the promoter surface density at the optimum values obtained on precursors with lower surface areas. These Fe–Zn–Cu–K catalysts exhibit hydrocarbon productivities similar to or higher than those obtained on Co-based catalysts at low temperatures and a much weaker selectivity dependence on temperature and H_2/CO ratio than those typically observed on Co-based catalysts.

ACKNOWLEDGMENTS

This work was supported by the U.S. Department of Energy (DOE) under contract number DE-FC26-98FT40308. X-ray absorption data were collected at the Stanford Synchrotron Radiation Laboratory (SSRL), which is operated by the Department of Energy (DOE), Office of Basic Energy Sciences under contract DE-ACO3-76SF00515. The authors thank Bjorn Moden and Dario Pinna and Patrick DaCosta for their assistance with the acquisition of the X-ray absorption data. We also acknowledge helpful discussions with Burtron H. Davis of the University of Kentucky and with Stuart L. Soled of ExxonMobil Research and Engineering.

REFERENCES

1. Dry, M. E., The Fisher–Tropsch synthesis, *in* "Catalysis-Science and Technology" (J. R. Anderson and M. Boudart, Eds.), Vol. 1, p. 160, Springer Verlag, New York, 1981.
2. Brady, R. C., and Pettit, R., *J. Am. Chem. Soc.* **103**, 1287 (1981).
3. Schulz, H., *Appl. Catal. A* **186**, 3 (1999).
4. Li, S., Meitzner, G. D., and Iglesia, E., *J. Phys. Chem. B* **105**, 5743 (2001).
5. Li, S., Li, A., Krishnamoorthy, S., and Iglesia, E., *Catal. Lett.* **77**, 197 (2001).
6. Soled, S. L., Iglesia, E., Miseo, S., DeRites, B. A., and Fiato, R. A., *Topics in Catal.* **2**, 193 (1995).
7. Habermehl, R., and Atwood, K., *Am. Chem. Soc. Div. Fuel. Chem. Prepr.* **8**, 10 (1964).
8. Vannice, M. A., *J. Catal.* **37**, 462 (1975).
9. Iglesia, E., Soled, S. L., Fiato, R. A., and Via, G. H., *J. Catal.* **143**, 345 (1993).
10. Iglesia, E., *Appl. Catal. A* **161**, 59 (1997).
11. Lide, D. R., and Frederikse, H. P. R. (Eds.), *in* "Handbook of Chemistry and Physics," 75th ed., pp. 6–151. Chemical Rubber Company Press, Boca Raton, FL, 1994.
12. Scherer, G. W., *J. Am. Ceram. Soc.* **73**, 3 (1990).
13. Miller, J. B., Rankin, S. E., and Ko, E. I., *J. Catal.* **148**, 673 (1994).
14. Schneider, M., Maciejewski, M., Tschudin, S., Wokawn, A., and Baiker, A., *J. Catal.* **149**, 326 (1994).
15. Iglesia, E., Soled, S. L., Baumgartner, J. E., and Reyes, S. C., *J. Catal.* **153**, 108 (1995).
16. Amelse, J. A., Butt, J. B., and Schwartz, L. H., *J. Phys. Chem. B* **82**, 558 (1978).
17. WinXAS97 is an XAS data analysis program for PCs running MS-Windows by Thorsten Ressler (http://ourworld.compuserve.com/homepages/t_ressler).
18. Malinowski, E. R., and Howery, D. G., *in* "Factor Analysis in Chemistry." Wiley, New York, 1981.
19. Meitzner, G. D., and Huang, E. S., *Fresenius J. Anal. Chem.* **342**, 61 (1992).
20. Madon, R. J., and Iglesia, E., *J. Catal.* **139**, 576 (1993).
21. Li, S., Ding, W., Meitzner, G. D., and Iglesia, E., *J. Phys. Chem. B.* **106**, 85 (2002).
22. Soled, S. L., and Iglesia, E., unpublished results.
23. Li, A., Li, S., and Iglesia, E., unpublished results.
24. Van der Laan, G. P., and Beenackers, A. A. C. M., *Ind. Eng. Chem. Res.* **38**, 1277 (1999).
25. Raje, A. P., and Davis B. H., *Catal. Today* **36**, 335 (1997).
26. Raje, A. P., O'Brien, R., and Davis, B. H., *J. Catal.* **180**, 36 (1998).
27. Mauldin, C. H., U.S. Patent No. 4,670,475 (1987).